Journal of Physics: Conference Series **336** (2011) 012018 doi:10.1088/1742-6596/336/1/012018

Dynamical probes of pairing correlations: two-particle transfer and two-particle break-up reactions

Ilyas Inci[1], Francisco Perez-Bernal[2] and Andrea Vitturi[3,4]

[1] Department of Physics, Akdeniz University, Antalya, Turkey
[2] Facultad de Ciencias Experimentales, Departamento de Fisica Aplicada, Universidad de Huelva, Huelva, Spain
[3] Dipartimento di Fisica G.Galilei, Via Marzolo 8, I-35131 Padova, Italy
[4] Istituto Nazionale Fisica Nucleare, Sezione di Padova, Via Marzolo 8, I-35131 Padova, Italy

E-mail: vitturi@pd.infn.it

Abstract. We investigate the role played by pairing correlations in two typical classes of nuclear reactions specifically involving pairs of particles: two-particle transfer reactions, where a pair of nucleons is exchanged between the reaction partners, and two-particle break-up reactions, where a pair of nucleons is emitted. In both cases we find that, although the process is mainly induced by the repeated action on each particle by the one-body field created by the reaction partner, a coherent enhancing effect is generated by the pair correlation present in the initial wave function, acting during the process and again present (in the case of two-particle transfer) in the final wave function. In the case of reactions involving weakly-bound nuclei the low-density features characterizing the vicinity of the drip line and the suggested consequent enhancement of the pairing correlations should show up as clear signature in both processes. From the point of view of their theoretical description, the vicinity of the drip lines will involve heavily the continuum part of the spectrum and we will test in simple models the validity of different discretization procedures used in the description of both structure and reaction.

1. Pairing correlations and two-particle trasfer proceeses

Two-particle transfer processes induced by light ions (reactions as (t,p), (p,t), (^{3}He,n), (α,d)) or heavy ions are considered the ideal tool to study the dynamical effects of pairing correlations. All these reactions do explore precisely the radial properties of pair correlations. Unfortunately, the situation is different, for example, from low-energy one-step Coulomb excitation, where the excitation probability is directly proportional to the B(Eλ) values. Here the reaction mechanism is much more complicated and not well established, so that the possibility of extracting spectroscopic information on the pairing field is not obvious.

It is often assumed that the cross section for two-particle transfer will scale with the square of the matrix element of the pair creation (or removal) operator. In this perspective in order to define and measure the collectivity of pairing modes one could compare with single-particle pair matrix elements to define some pairing single-particle units and therefore pairing enhancement factors. But the two-particle transfer process in not sensitive to just the pair matrix element. We have to look at the radial dependence of the pair transition density, which is relevant for the

reaction mechanism associated with pair transfer processes. As examples we show in figures 1 and 2 the comparison with pure single-particle configurations in the case of the addition mode around ^{16}O (i.e. the ground state of ^{18}O) and the removal mode around ^{208}Pb (i.e. the ground state of ^{206}Pb). The comparison is done in figure 1 directly on the local transition density ($\delta\rho_P(r,r)$). In figure 2 the comparison is done on the non-local transition density $\delta\rho_P(r_1,r_2)$ by fixing the position on one particle and plotting as contour plots in space the probability of finding the second one. One immediately sees that while for pure configuration one has equal probablity of finding the second particle on the same or on the opposite side with respect to the core, the pairing correlation induces a correlation in space, favouring the clustering of the pair.

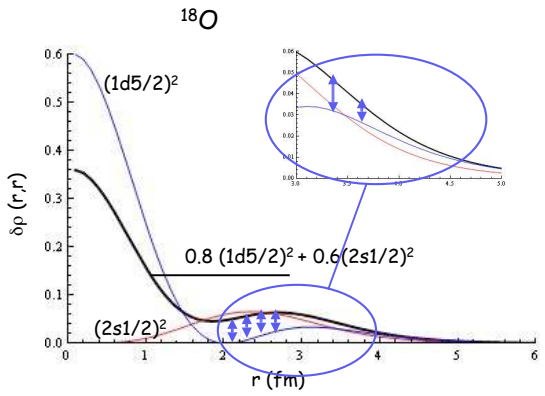

Figure 1. (Color online) Pair transition density in ^{18}O. The cases of pure $(1d5/2)^2$ and $(2s1/2)^2$ are compared with the case of correlated wave function.

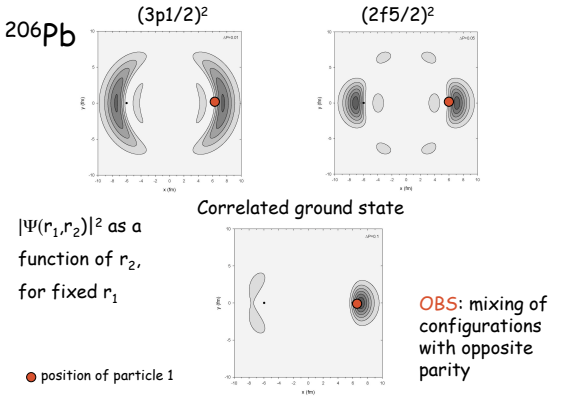

Figure 2. (Color online) Squared wave functions for the ground state of ^{206}Pb, plotted fixing the position of one particle as a function of the position of the second one. Pure configurations are compared with the case of pairing correlated wave function

One can see from these simple examples that the effect of the pairing on the spatial properties of the pair densities is clearly established. The difficult point is to clarify how the structure properties enter into the reaction mechanism. To this end one needs reliable models for the description of the reaction mechanism. There are actually in the literature a large number of different approaches, all trying to reduce the actual complexity of the problem, which is a genuine four-body scattering (the two cores plus the two transferred particles). Note also that different approaches are used in the case of heavy-ion induced reactions (where one may need detailed information on the wave functions in both target and projectile, but on the same time the reaction is mainly surface-peaked and semiclassical descriptions may apply) and in the case of light ions (as (p,t) reactions).

As an example, in a semi-microscopic approach the reaction mechanism is described as a one-step di-neutron (cluster) transfer. In this case the microscopy amounts to construct a formfactor obtained by double-folding the microscopic pair transition densities of initial and final states with some nucleon-nucleon interaction or by simple folding of microscopic pair density in the target with the one-body mean field of the projectile. Such an approach only involves the local transition densities and does not exploit the full non-local features of the pair correlation.

A fully microscopic approach is instead the one in which the two-particle transfer reaction is described by sequential two-step process (at each step one transfers one particle)[1, 2, 3]. In this case the pairing enhancement comes from the coherent interference of the different paths through the different intermediate states in (a-1) and (A+1) nuclei, due to the correlations in initial and

final wave functions. Basis ingredients of the calculation are the individual formfactors for one-particle transfer and the microscopic pairing correlated wave functions. Since such fully quantal calculations are rather complex (taking into account full recoil), semiclassical approximation scheme are commonly used (although with approximate treatment of recoil).

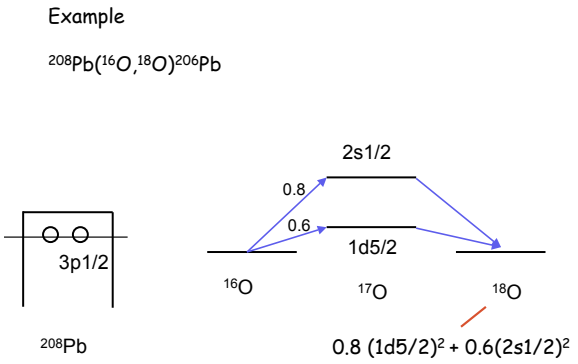

Figure 3. (Color online) Scheme of two-particle transfer etc in ^{18}O.

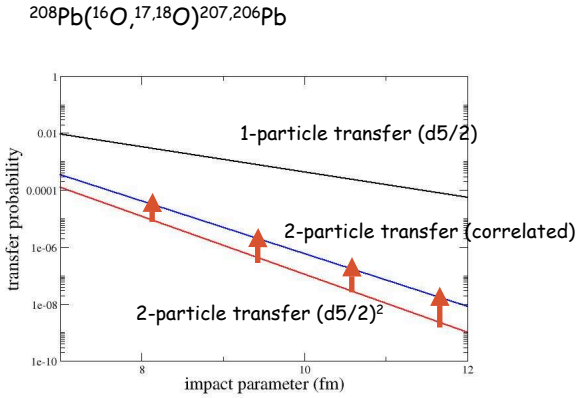

Figure 4. (Color online) Probabilities for one-, two- (uncorrelated) and two-particle (correlated) transfer as a function of the impact parameter

As an example, we consider the two-particle transfer reaction ^{208}Pb(^{16}O, ^{18}O$_{gs}$)^{206}Pb$_{gs}$ at a bombarding energy around the Coulomb barrier. We assume that the two particles are trasferred from the 3p1/2 level in ^{208}Pb into a correlated ground state of ^{18}O, taken as a linear combination of $(1d5/2)^2$ and $(2s1/2)^2$ (see figure 3). The effect of the correlation on the two-particle transfer probability is evident from figure 4, where the probabilities for one and two=particle transfer are shown as a function of the impact parameter. The results for the correlated case is compared with the corresponding values for the uncorrelated one in which the two particles are simply trasferred in pure $(1d5/2)^2$ orbits. Integrating over the impact parameter one obtains a two-particle transfer cross section which is approximately a factor two enhanced with respect to the uncorrelated case (3.90 mb with respect to 1.98 mb in the case of pure $(1d5/2)^2$ case).

As we move closer or even beyond the drip lines the previous picture is inevitably modified. As schematically shown in figures 5-6, we move from a situation in which all relevant intermediate states are bound (figure 5), to situations in which only part of these states are bound (figure 6), finally even reaching at the drip line situations in which no bound intermediate states are present and only due to the pairing interaction the (A+2) system becomes bound. Typical examples are given by the so-called Borromean nuclei such as ^{11}Li or ^{6}Li whose grond states are bound in spite of no available bound states in ^{10}Li or ^{5}He. For weakly-bound systems at the drip lines it is therefore mandatory to include in the models the positive energy part of the spectrum. If one wants to still use the same machinary used with bound states, one has to resort to the so-called discretization of the continuum. We will discuss this point in section 3.

2. Dineutron correlation and breakup reaction within a simple model: two-neutron halo nuclei in one dimension

Among neutron-rich nuclei, two-neutron halo nuclei are particularly intriguing systems to study. Their structure has often been described as a three-body system consisting of two valence neutrons interacting with each other and with the core nucleus. Some light neutron-rich nuclei,

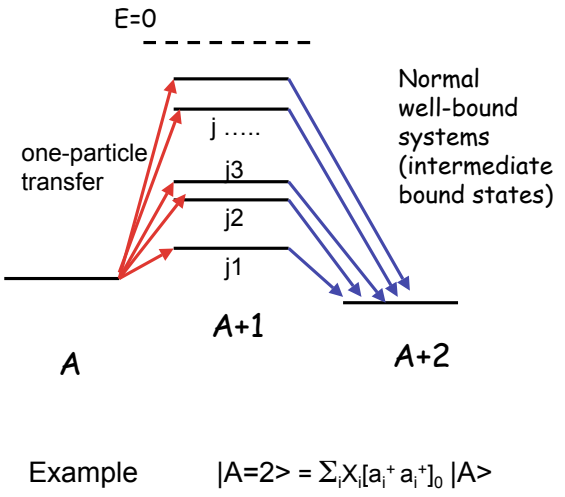

Figure 5. (Color online) Scheme of two-particle transfer for normal systems

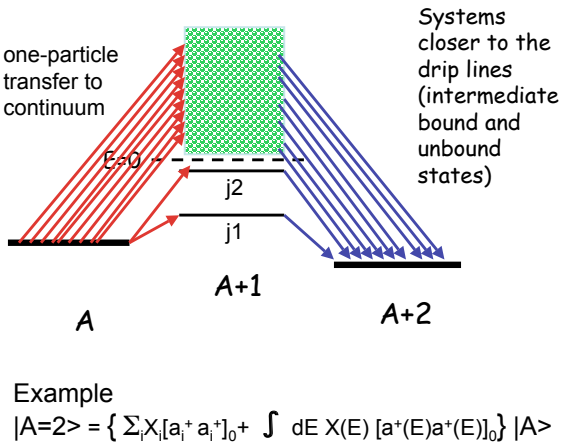

Figure 6. (Color online) Scheme of two-particle transfer for systems towards the drip line

such as ^{11}Li and ^{6}He, do not have a bound state in the two-body subsystem with a valence neutron and a core nucleus. These nuclei are referred to as Borromean nuclei, and their properties have been studied extensively both experimentally and theoretically . Nuclear breakup reactions of Borromean nuclei have also been investigated by the continuum-discretized-coupled-channels (CDCC) method and by the eikonal method

One of the most important current open questions concerning the Borromean nuclei is to clarify the characteristic nature of correlations between the two valence neutrons, which do not form a bound state in the vacuum. A strong dineutron correlation, where the two neutrons take a spatially compact configuration, has been theoretically predicted [4, 5, 6, 7, 8, 9, 10, 11] . Although the recent experimental observation of the strong low-lying dipole strength distribution in the ^{11}Li nucleus has provided an experimental signature of the existence of dineutron correlation in this nucleus, its direct evidence has not yet been obtained.

As discussed previously, the pair transfer reaction is another promising way to probe the dineutron correlation, as the cross section is known to be sensitive to the pairing correlation. However, as seen above, the reaction dynamics and the role of dineutron in the pair transfer reaction are rather complicated[12, 13, 14]. Apparently, it is urged to construct a theoretical framework for pair transfer which fully takes into account the pairing correlation and the dineutron correlation in its consequence.

We use here a simple toy model for two-neutron halo nuclei. Albeit its schematic nature, such model is rather useful as it allows detailed studies on the static and dynamical properties of two-neutron halo nuclei. A schematic model is also useful to deepen our understanding of two-neutron halo nuclei by providing intuitive pictures of several dynamical processes. To this end, we consider a three-body model in which the motion of two valence neutrons is confined within one-dimensional spatial space. The neutrons are assumed to move in a one-dimensional Woods-Saxon potential, while interacting with each other via a two-body interaction, which we take a density-dependent contact interaction [5, 15, 7, 16]. Denoting the coordinate of the two neutrons by x_1 and x_2, the three-body Hamiltonian reads,

$$H = -\frac{\hbar^2}{2m}\frac{d^2}{dx_1^2} + V(x_1) - \frac{\hbar^2}{2m}\frac{d^2}{dx_2^2} + V(x_2) + v_{nn}(x_1, x_2), \quad (1)$$

where m is the nucleon mass. Here, we neglect for simplicity the recoil kinetic energy of the

core nucleus. $V(x)$ is the neutron-core potential, which we take the Woods-Saxon form[23],

$$V(x) = -\frac{V_0}{1+e^{(|x|-R)/a}} \tag{2}$$

while v_{nn} is the neutron-neutron interaction. We take the density-dependent contact interaction for it, that is,

$$v_{nn}(x,x') = -g\left(1-\frac{1}{1+e^{(|x|-R)/a}}\right)\delta(x-x'), \tag{3}$$

where we assume that the density is given by the same functional form as the mean-field potential, Eq. (2). This is the so called surface type pairing interaction, which almost vanishes near the center of the core nucleus at $x \sim 0$. The density-dependent contact interaction has been successfully employed in the Hartree-Fock-Bogoliubov calculations for neutron-rich medium-heavy and heavy nuclei [9, 17] , as well as in describing the structure of ^{11}Li and ^{6}He nuclei with the three-body model [5, 15, 7] .

In order to obtain the ground state wave function of the two-neutron halo nucleus, we first solve the Schrödinger equation for the two-body subsystem,

$$\left[-\frac{\hbar^2}{2m}\frac{d^2}{dx^2}+V(x)-\epsilon_n\right]\phi_n(x)=0. \tag{4}$$

Each eigenstate n is assumed to have a two-fold degeneracy, depending on the direction of the spin of neutron. The continuum states are discretized by putting the nucleus within a large box. Denoting the size of the box to be $X_{\rm box}$, we impose the vanishing boundary condition $\phi_n(x)=0$ at $x=\pm X_{\rm box}$.

We expand the two-particle wave function $\Psi(x_1,x_2)$ with the single-particle wave functions $\phi_n(x)$ as

$$\Psi_{\rm gs}(x_1,x_2) = \sum_{n\le n'}\alpha_{nn'}\,\frac{1}{\sqrt{2(1+\delta_{n,n'})}}\left[\phi_n(x_1)\phi_{n'}(x_2)+\phi_n(x_2)\phi_{n'}(x_1)\right]|S=0\rangle. \tag{5}$$

Here we have assumed that the spin of the two neutrons form the total spin of S=0 configuration, so that the wave function is symmetric with respect to the interchange of x_1 and x_2. Notice that the Hamiltonian (1) conserves the parity. Since the ground state has positive parity, the expansion in Eq. (5) can therefore be restricted to the configurations where the states n and n' have the same parity. The expansion coefficients $\alpha_{nn'}$ are determined by diagonalizing the Hamiltonian matrix. Once the ground state wave function $\Psi_{\rm gs}(x_1,x_2)$ is obtained, the two-particle density $\rho_2(x_1,x_2)=|\Psi_{\rm gs}(x_1,x_2)|^2$ can be constructed. We now apply the one-dimensional model to a weakly-bound two-neutron halo nucleus. To this end, we take $R=1.27\times 9^{1/3}$ fm, $V_0=-50.085$ MeV, and a=0.67 fm for the Woods-Saxon potential, Eq. (2), in order to mimic the ^{11}Li nucleus. This potential possesses four bound single-particle states. We assume that the lowest three bound states are already occupied by the neutrons in the core nucleus, and exclude those states explicitly from the expansion in Eq. (5). In this way, the Woods-Saxon potential has effectively only one bound state with odd parity at $\epsilon_{\rm WS}=-0.15$ MeV. That is, the three-body system is bound by 0.3 MeV without the pairing interaction. We then include the pairing interaction. It is well known that a contact interaction has to be supplemented with an energy cutoff, $E_{\rm cut}$. We arbitrarily take here the cutoff energy to be 30 MeV, and we have fixed the pairing strength g to the value -12.35 MeV$\cdot$ fm in order to obtain a correlated ground state energy $E_{\rm g.s.}=-1$ MeV.

Figure 7 (a) shows the two-particle density of the ground state. The density distribution is largely concentrated along the line of $x_1 \sim x_2$, that is nothing but the manifestation of strong

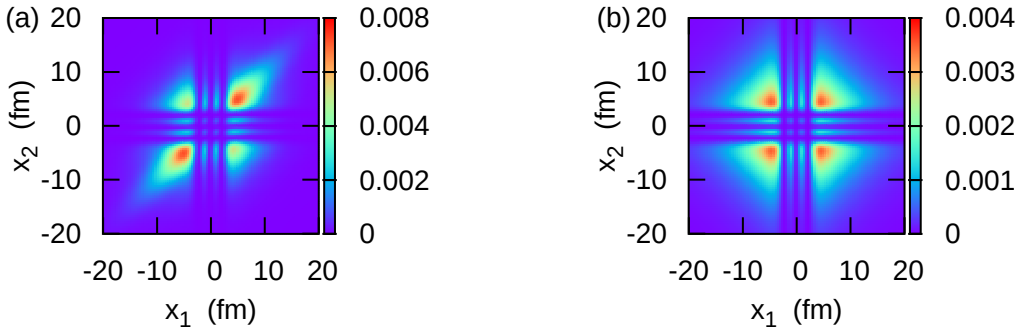

Figure 7. (Color online) The two-particle density for the correlated (left) and the non-correlated (right) ground states of a one-dimensional three-body model.

dineutron correlation discussed in Refs.[5, 6, 7, 8, 9, 10, 11]. The correlation largely hinders the density along the $x_1 = -x_2$ line, and only the peaks along $x_1 \sim x_2$ survive. When the pairing interaction is switched off, the two-particle density becomes that shown in figure 7 (b). The density for the non-correlated ground state is symmetric with respect to the transformation of $x_1 \to -x_1$ ($x_2 \to -x_2$) for a fixed value of x_2 (x_1), and it has therefore four symmetric peaks. See Refs. [18, 19, 20, 21, 22] for similar figures for ^{11}Li and other heavier nuclei.

Let us next discuss the time evolution of the two-particle wave function in the presence of an external field acting on each particle. As the external field, we take [23]

$$V_{\rm ext}(x_1, x_2, t) = \sum_{i=1,2} V_c\, e^{-t^2/2\sigma_t^2} e^{-(x_i - x_0)^2/2\sigma_x^2}, \tag{6}$$

with the parameters of V_c=3 MeV, $\sigma_t = 2.1\hbar$/MeV, and σ_x=2.2 fm. In order to investigate the time evolution, we solve the time-dependent two-particle Schrödinger equation,

$$i\hbar \frac{\partial}{\partial t} \Psi(x_1, x_2, t) = [H + V_{\rm ext}(x_1, x_2, t)] \Psi(x_1, x_2, t), \tag{7}$$

with the initial condition of $\Psi(x_1, x_2, t_0) = \Psi_{\rm gs}(x_1, x_2)$ at the initial time t_0. We orthonormalize the wave function to the occupied states using the projection procedure at each time step during the time evolution. In the calculations shown below, we take $ct_0 = -400$ fm, and use the implicit method [24] for the time propagation. We consider the symmetric perturbation, that is, $x_0 = 0$ in Eq. (6). We have confirmed that our conclusions remain qualitatively the same (except for the asymmetry in the two-particle density distribution along the $x_1 = x_2$ line) even if we choose an asymmetric perturbation [23], *e.g.,* with $x_0 = 2$ fm.

Figures 8(a), 8(b), 8(c), and 8(d) show the two-particle density at $ct = -400, 0, 300$, and 600 fm, respectively. As the time evolves, the extension of the peaks along the $x_1 = x_2$ line increases significantly. This is in marked contrast to the uncorrelated case shown in figures 9(a), 9(b), 9(c), and 9(d). In the uncorrelated case, the two-particle density expands democratically, indicating that there is the equal probability of emission of the two neutrons in the opposite directions to that in the same direction.

One can clearly see that due to the correlation the two neutrons fly apart from the core nucleus by sticking to each other due to the final state interaction. The effect of the correlation is clearly evidenced by the comparison with the uncorrelated case. We point out that both

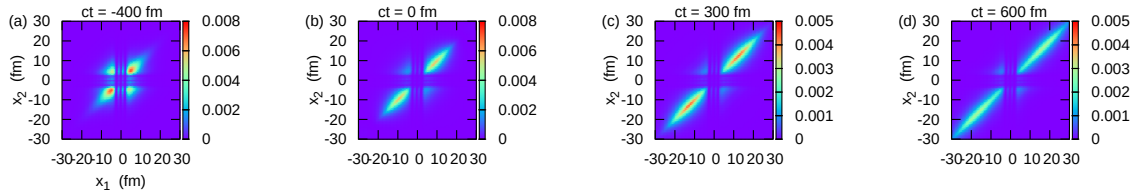

Figure 8. (Color online) The time evolution of the two-particle density. figures 8(a), 8(b), 8(c), and 8(d) show the two-particle density, $|\Psi(x_1, x_2)|^2$ at $ct = -400, 0, 300$, and 600 fm, respectively. Notice the difference scales among figures 8(a), 8(b), 8(c), and 8(d).

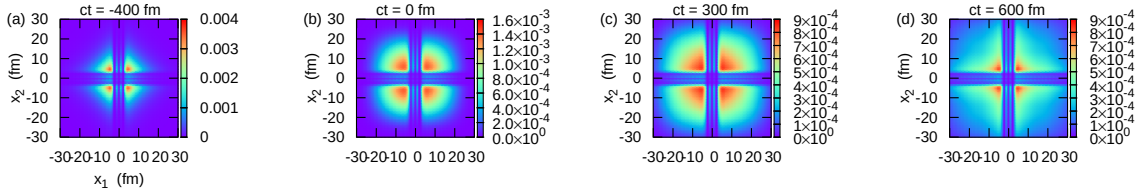

Figure 9. (Color online) Same as figure 8, but for the uncorrelated case with a vanishing neutron-neutron interaction. Notice the difference scales among figures 9(a), 9(b), 9(c), and 9(d).

the dineutron correlation in the ground state, as well as the neutron-neutron interaction acting during the time evolution (that is, the final state interaction) are important for the dineutron emission process.

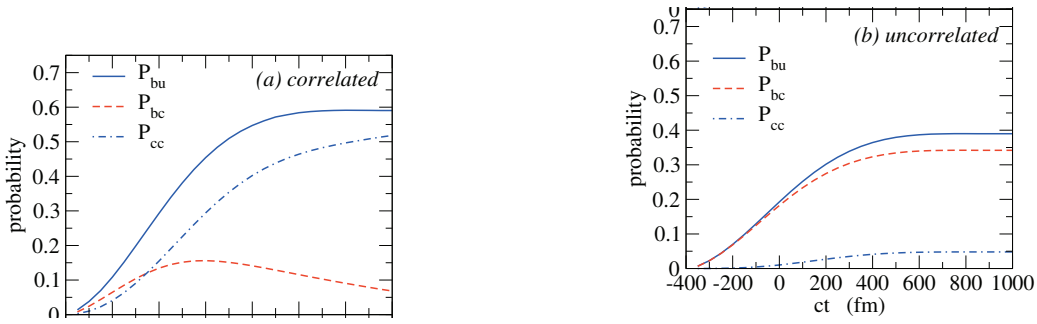

Figure 10. (Color online) The breakup probability as a function of time. The left and the right panels correspond to the correlated and the uncorrelated cases, respectively. The solid line shows the total breakup probability, while the dashed and the dot-dashed lines correspond to decompositions of the breakup probability into the (bc) (only one particle into the continuum) and (cc) (both particles into the continuum) processes, respectively.

The total breakup probability as well as the probability for each breakup process are shown in figure 10 as a function of time. The probabilities $P_{(bc)}$ and $P_{(cc)}$ correspond to the processes in which one or both particles are promoted to the continuum, respectively. The three probabilities (total, (cc) and (bc)) are denoted by the solid, the dashed, and the dot-dashed lines,

respectively. The left and the right panels correspond to the correlated and the uncorrelated cases, respectively. By comparing the two panels of figure 10, one finds that the total breakup probability is increased due to the pairing correlation. This is the case especially for $P_{\rm cc}$, that is, for the two-neutron emission process.

One also sees that the (bc) component first increases as a function of time while the increase of the (cc) component is somewhat delayed. For the correlated case, the (bc) component eventually decreases and the (cc) component takes over. This is a manifestation of the dominance of a sequential mechanism in the two-neutron breakup, if one intends to use a terminology of perturbation theory. Nevertheless, the strong final state interaction makes the dineutron-like emission the main breakup process as shown in figure 8.

In Ref. [25], it has been pointed out that the properties of the two-body subsystem with a neutron and the core nucleus play a decisive role in the Coulomb breakup of ^{11}Li and ^{6}He nuclei. This is because the external field is so weak for the Coulomb breakup that only one of the neutrons makes a transition to other (continuum) single-particle states. This corresponds to the (bc) process in our example. The external field is much stronger for the nuclear breakup process, and the two-step process, or even higher step processes, play an important role. This can be seen in a large probability for the (cc) process, $P_{\rm cc}$, shown in the left panel of figure 10. The effect of dineutron correlation can therefore be much easily seen in the nuclear breakup process as compared to the Coulomb breakup. A similar conclusion has been reached also in Ref. [26] (see also Ref. [27]).

3. Continuum discretization procedures

As discussed in the previous sections in the description of systems close to the drip lines the inclusion of continuum states becomes mandatory. Quite a variety of approaches have been developed to include continuum states in existing models, both in structure and reaction. Some of them are intrinsically devised to only include in the many-body wave functions components with at maximum one particle in the continuum, others are based on the use of complex eigenstates of the hamiltonian [28]. Most of the approaches, on the contrary, introduce the so-called discretization procedure [29]. In this case the continuum part of the single-particle spectrum is replaced by an alternative discrete sum of states with positive real energies, chosen according to different prescriptions. Examples are given by the expansion in Harmonic Oscillator basis, or similar as the Transformed Harmonic Oscillator, or the use of a large box where to impose vanishing boundary conditions.

As a simple example of the discretization procedure we consider again pure single-particle states in ^{17}O. We can from one side construct the exact $d_{5/2}$ and $s_{1/2}$ states, both bound (discrete) and unbound (continuum), generated by a Woods-Saxon potential and from the other side diagonalize the same potential in a Harmonic Oscillator basis (including up to either 20 or 34 major shells) . In the latter approach we obtain only discrete states, for both negative and positive energies, the latter states being dependent on the number of included HO shells. To check the validity of the discretization procedure, we compare in figure 11 the $B(E2)$ matrix elements from the bound $s_{1/2}$ state to all $d_{5/2}$ states. As apparent from the figure, one has nonvanishing matrix elements not only to the bound $d_{5/2}$ state, but also to the continuum part. By increasing the number of HO shells (and therefore incresing the density of the discrete states) the discrete calculation seems to tend to converge and to approach the true continuum values both in shape and in the integrated value. To check the effect of the possible presence of a resonant state at the continuum threshold, in figure 12 the Woods-Saxon potential has been reduced in order to move the $d_{5/2}$ state into the continuum. As clear from the figure, also in this case the $B(E2)$ continuum distribution is rather well reproduced (again in both shape and integrated value) by the discretized basis, as long as a large number of shells are included. Note

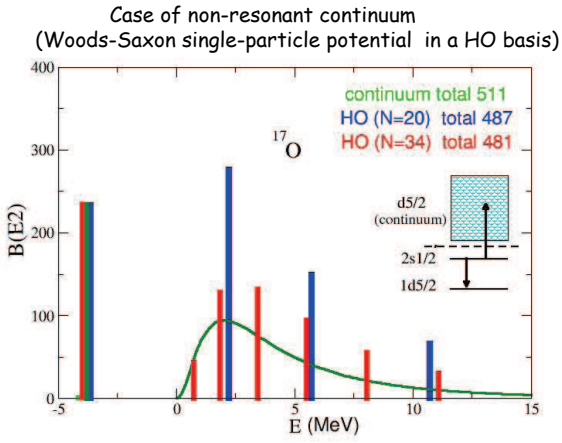

Figure 11. (Color online) $B(E2)$ matrix elements from the bound $s_{1/2}$ state to all $d_{5/2}$ states. Transitions to the true continuum states are compared with those obtained for the discretized states generated in HO basis.

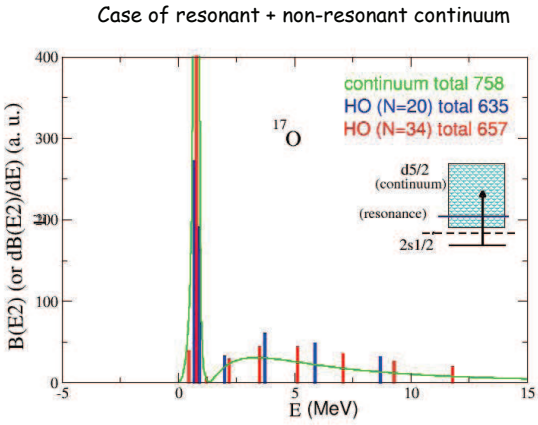

Figure 12. (Color online) Same as in figure 11, but with the one-body WS potential modified in order to have a resonant state close to the continuum threshold.

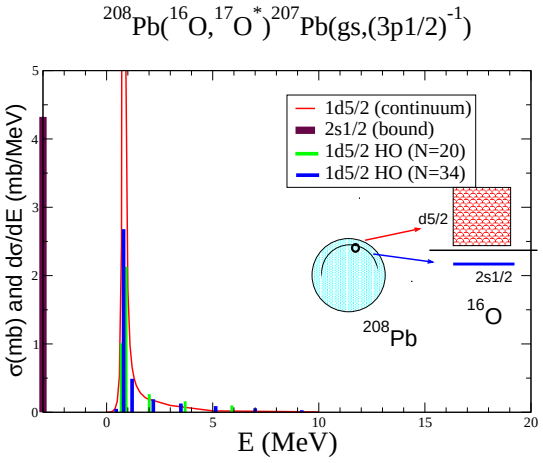

Figure 13. (Color online) Excitation function for one-particle transfer reaction ^{208}Pb(^{16}O, ^{17}O)^{207}Pb$_{gs}$ at a bombarding energy around the Coulomb barrier. We assume that the particle is trasferred from the 3p1/2 level in ^{207}Pb into the bound $(2s1/2)$ and the continuum $(1d5/2)$ states in ^{17}O. The total cross sections obtained with the true continuum states are compared with the results obtained with the discretized states

that in the $B(E2)$ matrix elements the presence of the initial bound $s_{1/2}$ wave function limits the relevant radial range for the integration to the nuclear volume, therefore cutting out the external region where the true continuum states display the characteristic oscillatory behaviour.

As a further test, we consider the one-particle transfer reaction ^{208}Pb(^{16}O, ^{17}O)^{207}Pb$_{gs}$ at a bombarding energy around the Coulomb barrier. We assume that the particle is trasferred from the 3p1/2 level in ^{207}Pb into the bound $(2s1/2)$ and the continuum $(1d5/2)$ states in ^{17}O. The total cross sections obtained with the true continuum states are compared in figure 13 with the

results obtained with the discretized states. Again, for a large number of HO shells, results seem to converge to the exact ones both in shape and magnitude. Note that the one-particle transfer process involves the construction of one-particle transfer formfactors where the final (bound or unbound) final wave function is folded with the initial bound state in ^{208}Pb, that again gives the largest contribution in the volume region.

All discretization procedures are equivalent as long as a full complete basis is used. In practice each procedure involves a number of approximations and truncations in the actual computations. Computational constraints may in fact become a severe problem, in particular when a large number of particles are allowed to move in the continuum. Comparing the positive and negative aspects of the different approaches is not an easy task, in view of the different sets of parameters that characterize each procedure. In addition the problem used as a test case may dispay such a complexity not to allow for an exact solution to be used as a reference for checking convergence procedures.

For these reasons we consider here the simplest many-body problem: particles moving in the one-dimensional mean field and two particles outside the core interacting via an additional density-dependent short range residual interaction [30, 31]. We will take a case in which the particles of the core fully occupy all the bound states and chose an interaction strength such as to produce a bound two-particle correlate state. The situation can therefore model the case of a two-particle halo nucleus (such as ^{6}He or ^{11}Li), which is bound in spite of the fact that the neighbour core+particle is unbound (as ^{5}He or ^{10}Li in the considered examples).

The one-body potential is assumed to be of the usual simple Woods-Saxon form $V(x) = -V_0 \,/\, (1 + \exp((|x| - R)/a))$ with parameters $V_0 = 12$ MeV, R=5 fm and a=0.8 fm. This potential admits three bound states at energies $-10.22, -6.00$ and -1.39 MeV, all supposed to be fully occupied. We have used different techniques to produce the (discrete) single-particle basis associated with this one-body potential. We compare here the results obtained by calculating the single-particle Woods-Saxon states using either a harmonic oscillator basis or a finite box at which to impose boundary condition of infinite well. The energies of the resulting states are shown in figure 14 as a function of the number of shells used in the HO basis and in figure 15 as a function of the box radius. Note the variation, in density and in energy, of the unphysical positive energy states.

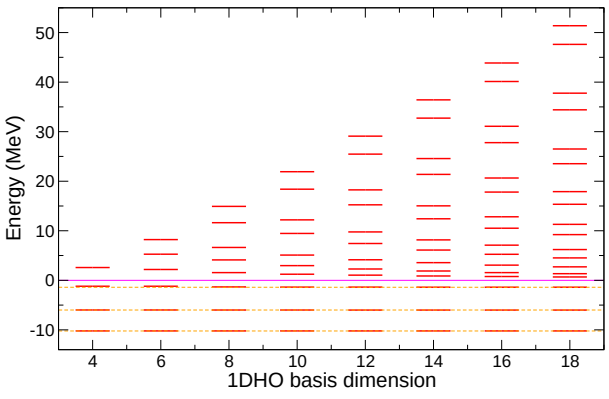

Figure 14. (Color online) Single particle energies obtained diagonalizing the WS one-body potential in a HO basis, for different values of the number of shells.

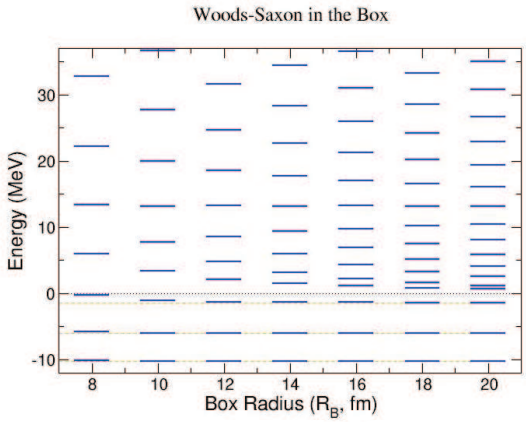

Figure 15. (Color online) Same as in figure 14, but diagonalizing the WS interaction in a finite box, for different values of the box radius.

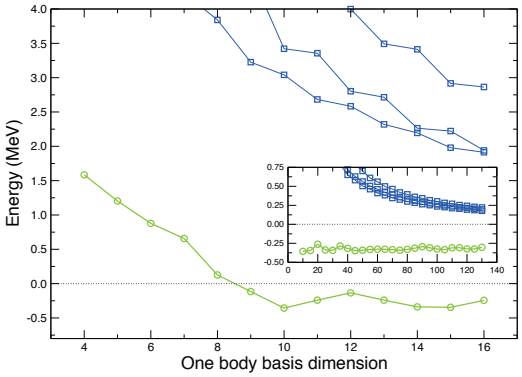

Figure 16. (Color online) Energies of the correlated two-particle states resulting from the diagonalization procedure. A Harmonic Oscillator has been as a basis to construct the WS single-particle states. In the abscissa is given the number of oscillator shells.

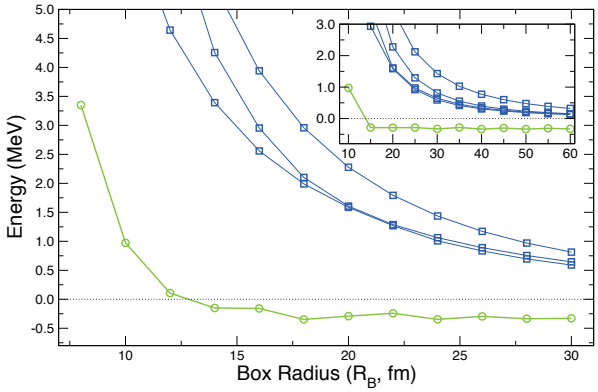

Figure 17. (Color online) Same as in figure 16, but with single-particle states obtained in a finite box, for different values of the box radius.

The residual interaction among the two additional particles is assumed of the form $V_{int}(x_1, x_2) = -V_{int}\ \delta(x_1 - x_2)\ \rho(x)$. We have diagonalized this residual interaction in the two-particle basis. Figures 16 and 17 show the energies of the resulting correlated states as a function of either the number of shells used in the HO basis or the box radius. Positive energy states have no physical meaning (dependent as they are from the chosen basis) but, as apparent from the figure, the residual interaction creates a (physical) bound state with a converging value of the energy (compare e.g. the inset in figure 16, where the number of shells oversizes one hundred or the inset in figure 17 where the box radius reaches 60 fm). A decent value of the energy can be achieved already with a dozen of HO shells or 15 fm for the box size. However, this is not sufficient to ensure a correct description of the resulting wave function. To check this point we display in figures 18 and 19 the correlated two-particle wave function (for $x_1 = x_2 = x$. As clear from the figure an extremely large number of shells (or a large box radius) has to be used to provide a proper behaviour in the tail region. Note that this behaviour is essential, for example, to describe properly the pairing field or the two-particle transfer processes in heavy-ion induced reactions.

The results of our analysis (only sketched here) shows how delicate is the problem of the discretization of the continuum in connection with reaction processes, where the tails of the wave functions may play a decisive role. A proper descrition of nuclear systems at the drip lines will therefore require further studies for both structure and reactions models.

Acknowledgments

This work presents results obtained in collaboration with Kouichi Hagino, Lorenzo Fortunato, Hiro Sagawa and Hugo Sofia. Important contributions on this subject have been obtained in these years by the Milano group, and the authors acknowledge fruitful discussions with Enrico Vigezzi, Francisco Barranco and Gregory Potel.

References

[1] Broglia RA and Winther A 1991 *Heavy-Ion Reactions: Lecture Notes*, Addison-Wesley, New York
[2] von Oertzen W and Vitturi A 2001 *Rep. Prog. Phys.* **64** 1247

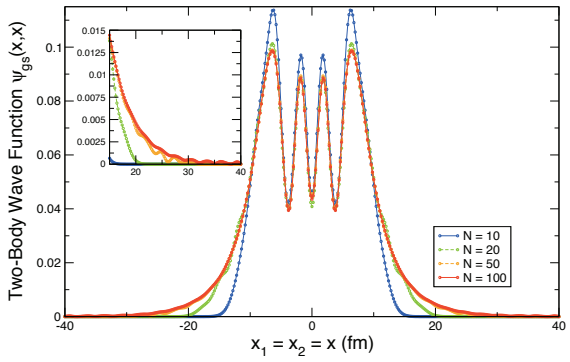

Figure 18. (Color online) Two-body bound state obtained after Hamiltonian diagonalization using a truncated one-body HO basis with number of shells 10, 20, 50, and 100.

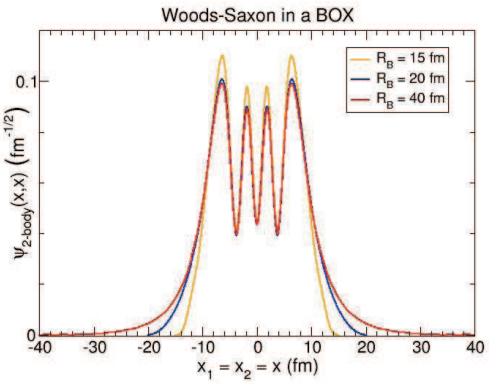

Figure 19. (Color online) Same as in figure 18, but with single-particle states obtained in a finite box, for values of the box radius 15, 20 and 40 fm.

[3] Potel G, Barranco F, Vigezzi E etal 2010 *Phys. Rev. Lett.* **105** 172502; Potel G, Marini F, Idini A, Barranco F, Vigezzi E, Broglia RA, http://arxiv.org/abs/1105.6250
[4] Hansen P G and Jonson B 1987 *Europhys. Lett.* **4** 409
[5] Bertsch G F and Esbensen H 1991 *Ann. Phys. (N.Y.)* **209** 327
[6] Zhukov M V, Danilin B V, Fedorov D V, Bang J M, Thompson I J, and Vaagen J S 1993 *Phys. Rep.* **231** 151
[7] Hagino K and Sagawa H 2005 *Phys. Rev. C* **72** 044321
[8] Hagino K, Sagawa H, Carbonell J, and Schuck P 2007 *Phys. Rev. Lett.* **99** 022506
[9] Matsuo M, Mizuyama K, and Serizawa Y 2005 *Phys. Rev. C* **71** 064326
[10] Pillet N, Sandulescu N, and Schuck P, 2007 *Phys. Rev. C* **76** 024310
[11] Matsuo M 2006 *Phys. Rev. C* **73** 044309
[12] Tanihata I *et al.* 2008 *Phys. Rev. Lett.* **100** 192502
[13] Chatterjee A *et al.* 2008 *Phys. Rev. Lett.* **101** 032701
[14] Lemasson A *et al.* 2009 *Phys. Rev. Lett.* **103** 232701
[15] Esbensen H, Bertsch G F and Hencken K 1997 *Phys. Rev. C* **56** 3054
[16] Hagino K and Sagawa H 2007 *Phys. Rev. C* **76** 047302
[17] Bender M, Heenen P.-H., and Reinhard P.-G. 2003 *Rev. Mod. Phys.* **75** 121
[18] Hagino K, Sagawa H, and Schuck P 2009 *Int. J. of Mod. Phys. E* **18** 2045
[19] Catara F, Insolia A, Maglione E, and Vitturi A 1984 *Phys. Rev. C* **29** 1091
[20] Ferreira L, Liotta R J, Dasso C H, Broglia R A and Winther A 1984 *Nucl. Phys. A* **426** 276
[21] Herzog M W, Civitarese O, Ferreira L, Liotta R J, Vertse T and Sibanda L J 1986 *Nucl. Phys. A* **448** 441
[22] Lotti P, Cazzola F, Bortignon P F, Broglia R A, and Vitturi A 1989 *Phys. Rev. C* **40** 1791
[23] Dasso C H and Vitturi A 2009 *Phys. Rev. C* **79** 064620
[24] Koonin S E, Davies K T R, Maruhn-Rezwani V, Feldmeier H, Krieger S J, and Negele J W 1977 *Phys. Rev. C* **15** 1359
[25] Hagino K, Sagawa H, Nakamura T, and Shimoura S 2009 *Phys. Rev. C* **80** 031301(R)
[26] Assié M and Lacroix D 2009 *Phys. Rev. Lett.* **102** 202501
[27] Assié M *et al.* 2009 *Eur. Phys. J. A* **42** 441
[28] Michel N, Nazarewicz W, Ploszajczak M, and Rotureau J, 2006 *Phys. Rev. C* **74** 54305; Hagen G, Jensen MH, and Michel N, 2006 *Phys. Rev. C* **73** 64307
[29] Tsukiyama K, Otsuka T and Fujimoto R 2009, *AIP Conf. Proc.* **1165** 59
[30] Pérez-Bernal F and Vitturi A 2009 *AIP Conf. Proc.* **1165** 305
[31] Vitturi A and Pérez-Bernal F 2010 *Nucl. Phys. A* **834** 428c